Directivity Analysis of Ultrasonic Waves on Surface Defects Using a Visualization Method

Young Hyun Nam*

(*Received June 22, 1998*)

Ultrasonic testing uses the directivity of the ultrasonic wave, which propagates in one direction. The directivity is expressed as the relationship between the propagation direction and its sound pressure. The directivity of an ultrasonic wave is related to the choice of probe arrangement, testing sensitivity and scanning pitch, and correct measurement of defect size and location. This paper investigated the directivity of ultrasonic waves, which are scattered from a slit defect located in simulated butt weld joint using a visualization method. When the defect size was smaller than the wavelengths, clear directivity in the reflected wave was observed. When the ratio of defect size to wavelength is greater than 1.5, measured directivities almost agree with the theoretical directivity. The directivity of shear waves scattered from the slit defect varied according to probe direction (Far defect, Near defect). The angle of reflection wave became similar to angle of incidence as the height of excess metal in welded joint increased.

Key Words: Butt Joint, Visualization, Directivity, Surface Defect, Ultrasonic Wave Testing

1. Introduction

For detecting and characterizing the defects in ultrasonic testing, it is important to know the directivity of ultrasonic waves emitted from angle probes and reflected from the defect. In ultrasonic testing, the directivity of ultrasonic waves is closely related to the testing sensitivity, the scanning pitch, the arrangement of probes, and the defect size and location (ASNT, 1991; Krant Kramer, 1990).

Since the sound pressure field in the solid cannot be measured directly, most studies on ultrasonic directivity have been carried out in the theoretical field assuming the continuous wave. The directivity of the probe is ordinarily measured by using a semi-cylindrical shape test block and an electrodynamic sensor. In this method, however directivity of wave propagation cannot be precisely measured, and there is no method able to measure the directivity of reflected waves at the defect. Moreover, the ultrasonic testing uses a pulse of an elastic wave in solid (Ludwig and Lord, 1986 ; Ogilvy, 1986a ; 1986b ; 1987 ; You and Lord, 1989 ; Ogilvy, 1992 ; Harumi, 1986).

We have developed an ultrasonic wave visualization system, based on the synthesized photoelastic method. The system has high sensitivity for ultrasonic wave visualization and measures the sound pressure distribution from the visualized ultrasonic waves quantitatively.

The purpose of this paper is to measure the directivity of the ultrasonic waves using the visualization method. We measured the directivity of shear waves reflected from surface defect and the directivity change with position of probe using the slit defect located in simulated butt joint made of pyrex glass. In the case of surface defect, these experimental results were compared with the theory, which was based on the continuous wave. The applicability of continuous wave theory was discussed in terms of the parameter d/λ, where d is defect size and λ is the wavelength.

* R & D center, Korea Heavy Industries & Construction CO., LTD.

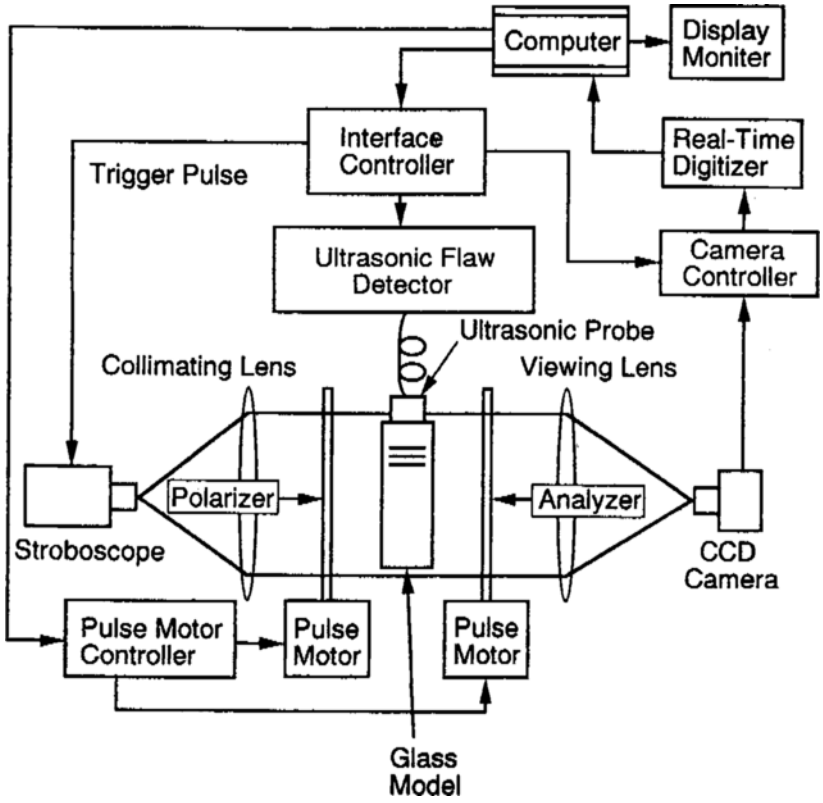

Fig. 1 Diagram of sound pressure visualization system.

2. Visualization System

The configuration of the ultrasonic visualization system used in this study is diagrammed in Fig. 1. The ultrasonic flaw detector, whose rate of repetition and synchronized output is 60 Hz, drives the ultrasonic probe to generate pulsed ultrasonic waves into the test piece, as is similar to the ultrasonic non-destructive testing. The system consists of a regular linear polariscope, having a stroboscopic light source, and a digital image-processing system for the photoelastic stress analysis (You and Lord, 1989 ; Ogilvy, 1992 ; Harumi, 1986). A commercial stroboscopic light source, giving a light flashing of very short duration (less than 200 ns), is positioned at the focal point of a collimating lens, whose effective diameter of field is 150 mm. Trigger pulses are sent from the interface controller to stroboscope, ultrasonic flaw detector and TV camera controller to synchronize with each other. The trigger pulse actuating the stroboscope provides the delay time against the trigger pulse of the ultrasonic flaw detector. By varying the delay time an observer can change the position at which the pulsed ultrasound is stroboscopically frozen and imaged.

The visualized images are obtained using Pyrex glass of 20 mm in thickness. Pyrex glass was used as a test piece because its ultrasonic wave velocities are similar to that of steel and it has a better stress-optical coefficient than most inorganic glasses.

Two visualized images with 45 degrees different polarizer orientation are synthesized in the image processing computer or conventional 35 mm camera, using double exposure technique in this case, to avoid the variation of visualized sensitivity with wave propagation direction relative to the orientation of incident polarized light. TV camera uses a high sensitivity vidicon television-camera

tube to visualize the ultrasonic wave in solid. The picture is divided into 512 lines and each line is divided into 512 parts. The brightness is converted into a video signal with 8-bit resolution. A display and a monitor visualize the information and act a graphics/numeric terminal for image processing, wave stress data analysis, program development and graphical data display. A computer has a special hardware for image processing to perform the stress field analysis in a short time.

3. Synthesized Photoelastic Method

When using linear polarized light, the visualized picture varies according to the change of the direction of polarizer's and analyzer's principal axis because the visualized image contains isoclinic lines. Figure 2 illustrates the brightness at any point when the same stress field is observed in the linearly polarized light. In this figure, I_1 is the intensity of the brightness at any point on the first picture and I_2 is on the second picture. In the case of synthesized picture, the intensity of the brightness at any point corresponds only to the principal stress difference. The relationship between the intensity of the brightness and the principal stress difference is the same as the case of the circular polarization obtained using quarter wave plates. But the sensitivity of the ultrasonic wave visualization using synthesized technique is much higher than that using circular polarized light. Since the relationship between principal stress components are well known as shown in Fig. 2, the ultrasonic wave stress (sound pressure) can be calculated from the measured intensity of the brightness on the synthesized picture. Synthesization of the first and second pictures was performed in the computer.

4. Directivity Analysis

Ultrasonic examination uses the directivity of the ultrasonic wave which propagates in a single direction. The directivity is expressed as the rela-

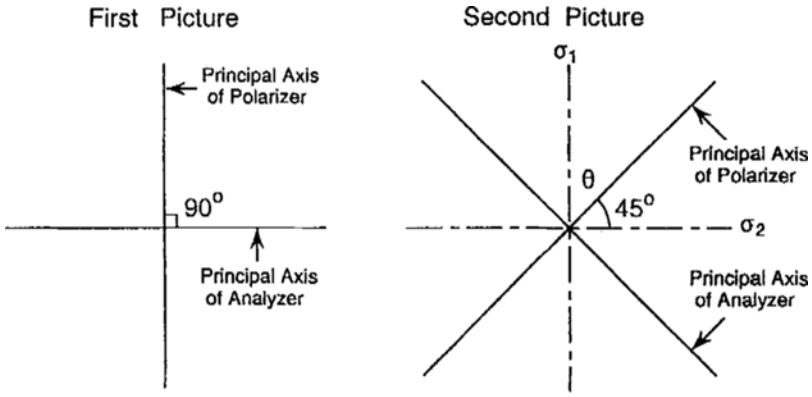

$I_1 = a^2 \cdot \sin^2 2\theta \cdot \sin^2 \delta/2$ $\qquad$ $I_2 = a^2 \cdot \cos^2 2\theta \cdot \sin^2 \delta/2$

$\delta = c \cdot d \cdot (\sigma_1 - \sigma_2)$ $\qquad$ σ_1, σ_2 : Principal Stress Value

C : Photoelastic Constant $\qquad$ d : Thickness of Test Piece

θ : Angle Between Direction of σ_1 and Principal Axis of Polarizer in First Picture

Synthesized Picture

$I = I_1 + I_2 = a^2 \cdot \sin^2 \delta/2$

Sound Pressure

Longitudinal Wave ---- σ_1 ($\sigma_2 = 0$)

Shear Wave ---------- σ_1 ($\sigma_2 = -\sigma_1$)

Fig. 2 Synthesized Photoelastic Method.

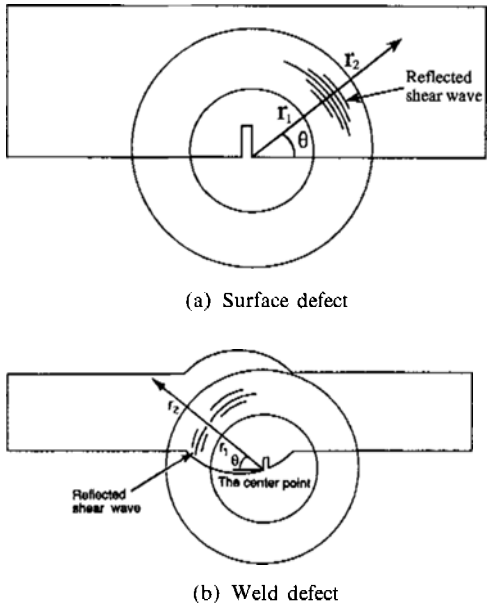

(a) Surface defect

(b) Weld defect

Fig. 3 Determination of directivity of ultrasonic wave.

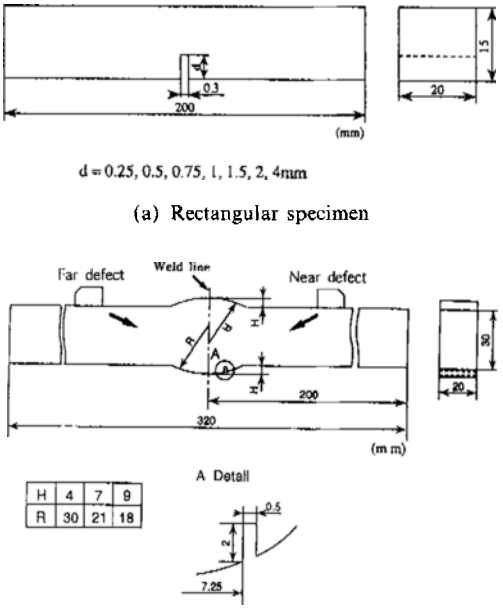

(a) Rectangular specimen

(b) Butt joint specimen

Fig. 4 Dimension of test specimen.

tionship between the propagation direction and its sound pressure.

Figure 3 schematically illustrates the manner by which directivity is determined from the visualized sound pressure image. We first located the center point of directivity from the circular curvature of the visualized shear wave. Next, we set two circles, which have radius of r_1 and r_2, from the center to fix the examination range of sound pressure in θ direction. This is specially important for the directivity analysis of reflected shear waves from the defect, because ultrasonic scattering from the defect produces many reflected waves and it is necessary to discriminate the wave to be analyzed. The directivities of the waves were obtained from the relationship between the angle θ and the maximum sound pressure value on the line from r_1 to r_2(Hall, 19847 ; Date et al., 1987 ; Date Udagaula, 1989).

5. Experimental Method

Figure 4 shows the dimensions of the test specimens used in this experiment. The specimens made of pyrex glass were used for ultrasonic visualization experiments, because it has better optical coefficient than inorganic glasses, small attenuation and sound velocity [longitudinal wave: 5,490 m/s, transverse wave: 3,420 m/s] very similar to that of the steel.

The actual refraction angle of angle probes in pyrex glass is measured by the visualization method. The transducer crystal size was always the same: 8×9 mm. The probe frequencies of 2 and 4 MHz were used. The probes had nominal refraction angle of 45 and 60 degrees for steel. Machine oil was used as acoustic couplant.

The thickness of the specimens was 20 mm. In the case of surface defect, the specimens had various slits ranging in depth from 0.25 to 4 mm. In the case of slit defect in simulated weld joint, the heights of excess metal are varied to 4, 7 and 9 mm.

For the measurement of directivity, we set the reflected shear wave after 12 and 20 mm propagation from the slit root. The directivity of the reflection wave was measured in two directions [Far defect, Near defect]. The far defect and near defect mean that the angle probes are located to the left and right side of the center line in the simulated butt weld, respectively as shown in Fig. 4. The maximum echo position means that probe

was put at the maximum echo height position from the defect.

6. Compared Theory to Directivity of Surface Defect

The internal crack-like defect was used to compare with the experimental result.

Reflected wave directivity $D_F(\alpha, \beta)$ (Ammirato, 1977) is:

$$D_F(\alpha, \beta) = 2d \cdot \cos\alpha \cdot \frac{\sin X_t}{X_t} \quad (1)$$

where $X_t = \frac{2\pi d}{\lambda}(\sin\beta - \sin\alpha)$ and λ is the wavelength.

In order to compare the internal crack-like defect with the surface slit, the surface slit depth was one-half the internal defect size "d". Validity of this correspondence was obtained in the perfect reflection of the shear wave at the bottom surface in the slit. This reflection occurred when we used the angle probe of 45 degrees. In the case of 60° angle probe, bottom reflection produces mode -conversion. Thus, we compared the directivity results obtained using angle probe of 45 degrees with the theoretical one, in which we set $\alpha = 45$ in Eq. (2).

7. Results and Discussion

7.1 Directivity of reflected shear waves from surface defect

Figures 5(a) and 5(b) show the visualized image and the directivity of shear wave reflected from the defect with slit depth of 1 mm. The probe was in maximum echo position, and the angles of reflected shear waves were 17 and 49 degrees, respectively.

Figure 6 shows the change of directivity with the slit depth and compared with the theoretical one. Note that there is sharp directivity in the case of small slit depth; d=0.5 mm, whereas weak directivity was predicted in the continuous theory.

(a) Visualized shear waves scattered at defect

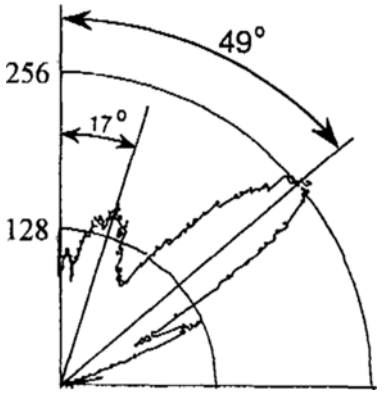

(b) Directivity

Fig. 5 Direcitivty of 2 MHz-45° shear waves reflected from surface defect.

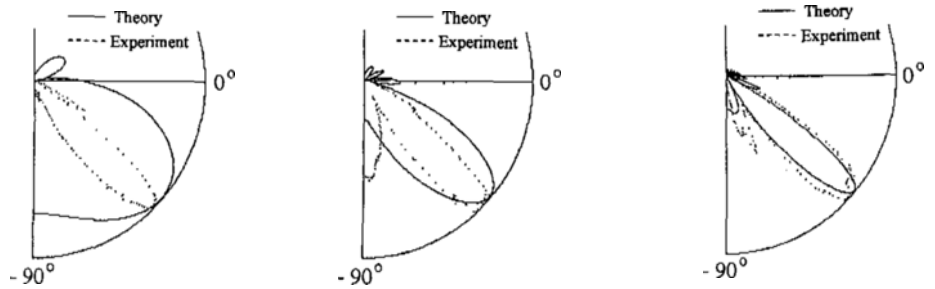

(a) d=0.5mm, d/λ=0.59 (b) d=1mm, d/λ=1.17 (c) d=2mm, d/λ=2.34

Fig. 6 Comparison of experimental directivity with theory for surface defects. Test frequency: 4 MHz.

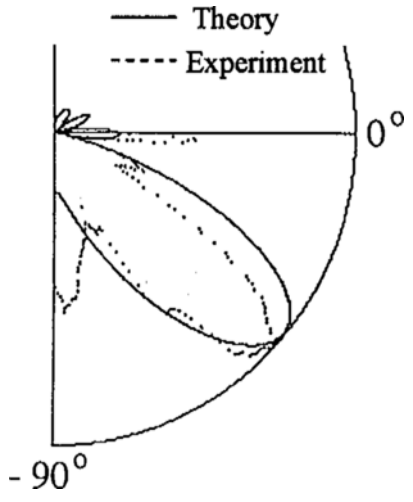

(a) d=2mm, d/λ=1.17

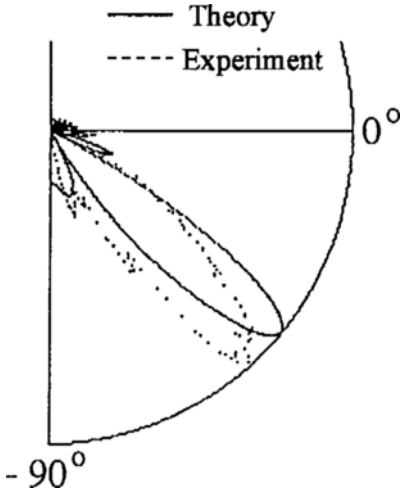

(b) d=4mm, d/λ=2.34

Fig. 7 Comparison of experimental directivity with theory for surface defects. Test frequency: 2 MHz.

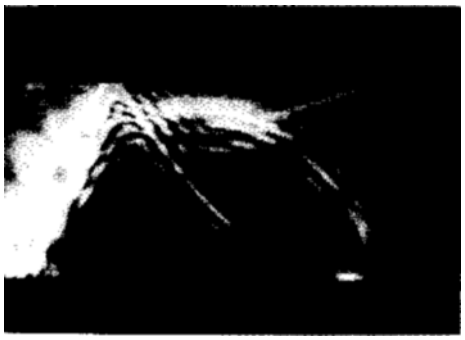

(a) Visualized shear waves scattered at defect

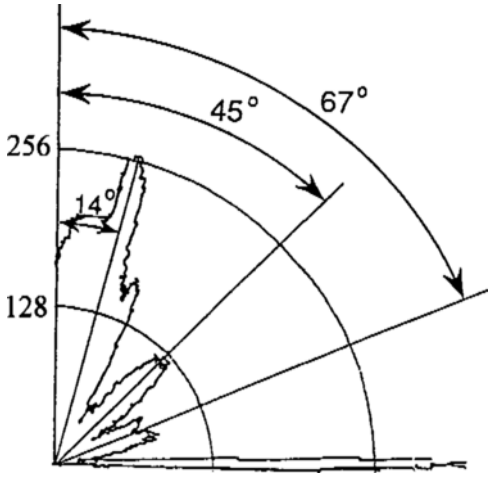

(b) Directivity

Fig. 8 Directivity of shear waves reflected from surface defect. Test frequency: 2 MHz, Refracted angle: 60 degrees, d=1 mm.

The difference between the theory and the experiment is considered to be due to the effect of pulse. The pulse contains the wide frequency component against the center frequency of the probe. In this case, the high frequency component of the pulse produces the sharp directivity as observed in the visualization experiments. In the case of large slit depth or large d/λ values as shown in Fig. 7, the experiment and theory are well agreed. Figures 6 and 7 represent that the same directivities [Fig. 5 (b) and Fig. 6(a), Fig. 5(c) and Fig. 6(b)] were obtained, when the parameters d/λ were the same.

Angle probes of 60 degrees produced complicated reflected waves from the slit as shown in Fig. 8. Three peaks of the directivity[main lobe: 14 degrees, side lobe: 45, 67 degrees] were observed due to the mode conversion at the reflection of the slit. When d/λ value is the same, the similar directivity of the single peak was also observed in probes as shown in Fig. 9.

The side lobe of the directivity is produced by the interference of the continuous wave. For example, a first side lobe is due to the retardation of one wavelength. This interference is possible only for a continuous wave. Pulse waves with single peaks do not produce the strong overlapping required to make the side lobe. From the

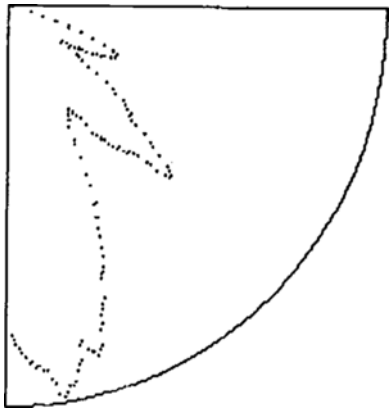

(a) 4MHz, d=1mm

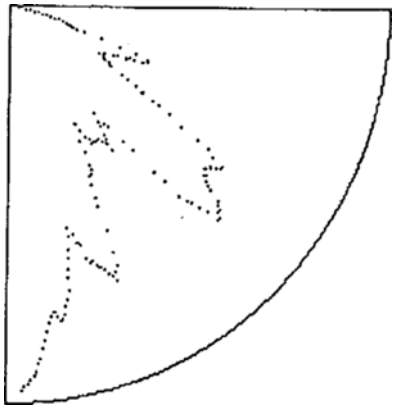

(b) 2MHz, d=2mm

Fig. 9 Directivity of shear waves reflected from surface defects. Refracted angle: 60 degrees $d/\lambda = 1.17$.

comparison of defect directivity analysis, theoretical directivity agreed well with the experimental results in the range of $d/\lambda > 1.5$. These results suggest that the continuous wave theory can be applied to the range of $d/\lambda > 1.5$.

7.2 Directivity of reflected shear wave from slit defect in base metal

Figure 10(a) shows the visualized image of reflected shear wave, having propagated distance of 12 mm from the slit root. The frequency of angle probe was 4 MHz, and the probe put the left side of weld line [far defect]. The incident wave was propagated from the upper left-hand to the bottom right-hand. In the visualized image, we can observe one reflected shear wave and one

(a) Visualized shear waves (H=4mm)

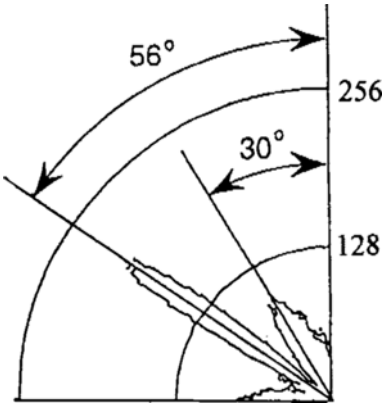

(b) Directivity

Fig. 10 Directivity of 4 MHz-60° shear waves reflected from far defect (Probe was at the maximum echo position).

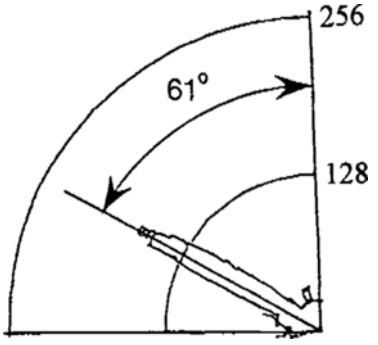

Fig. 11 Directivity of 4 MHz-60° shear waves reflected from near defect (H=7 mm).

surface wave [S] propagated according to surface of weld metal in welded joint. The height of excess metal in welded joint [H] was 4 mm. Figure 10(b) shows the directivity obtained from

(a) Visualized shear waves (H=9mm)

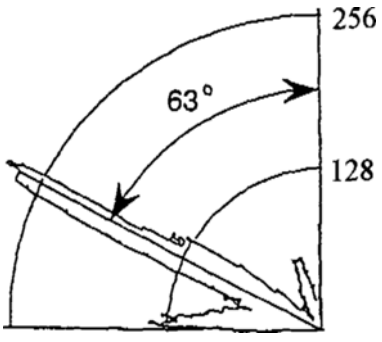

(b) Directivity

Fig. 12 Direcitivity of 4 MHz-60° shear waves reflected from far defect.

(a) Visualized shear waves (H=4mm)

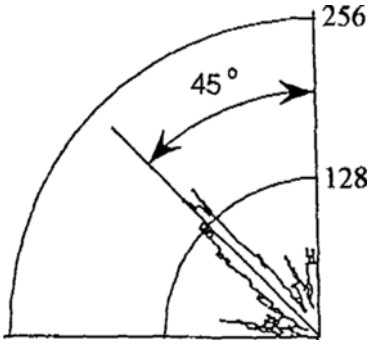

(b) Directivity

Fig. 13 Directivity of 4 MHz-60° shear waves reflected from near defect.

Fig. 10(a). The angle of reflected shear waves are 30 and 56 degrees.

Figure 11 shows the directivity of 4 MHz shear waves reflected from the defect. The angle of reflected shear wave is 61 degrees. The height of excess metal in welded joint [H] was 7 mm.

Figure 12 shows the visualized image and the directivity of 4 MHz shear waves reflected from the defect. The angle of reflected shear wave is 63 degrees. The height of excess metal in welded joint [H] was 9 mm. The behavior of reflected shear waves became simple with increasing the height of excess metal in welded joint, and the angle of reflected shear wave became similar to the angle of incidence. The directivity pattern of reflected shear waves were largely changed with the shape of welded joint, because the reflection at the slit defect became double reflection with increasing excess metal in welded joint.

Figure 13 shows the visualized image and the directivity of 4 MHz shear waves reflected from the near defect. The angle of reflected shear waves is 45 degrees. The height of excess metal in welded joint [H] was 4 mm. The intensity of reflected shear wave in far defect case was strong compared with that of near defect, because the reflected area to incident wave was large.

Figure 14 shows the visualized image and the directivity of 2 MHz shear waves reflected from the far defect. The angle of reflected shear waves are 16 and 55 degrees. The height of excess metal in welded joint [H] was 4 mm.

8. Conclusions

This paper studied the directivity of ultrasonic waves reflected from the defects by a visualization method. The following conclusions were obtained.

The sharp directivity existed in the slits smaller

(a) Visualized shear waves (H=4mm)

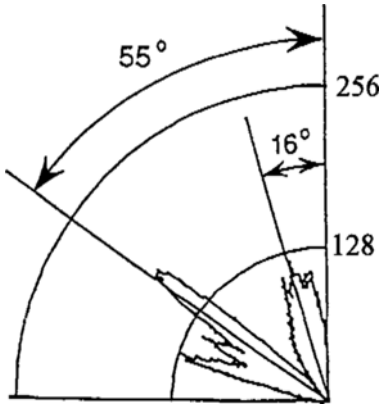

(b) Directivity

Fig. 14 Direcitivty of 2 MHz-60° shear waves reflected from far defect.

than the ultrasonic wavelength. The same directivities were obtained when the parameter d/λ was the same in the case of defect directivity. In the case of $d/\lambda > 1.5$, directivity of surface defect measured from the visualization agreed with the theoretical directivity. The directivity of shear waves reflected from slit defect were different according to probe direction [Far defect, Near defect]. A difference of directivity of reflection wave existed between 2 MHz and 4 MHz angle probes. The angle of reflection was become similar to angle of incidence as increasing the height of excess metal in welded joint.

References

Ammirato. F. V., 1977, "A Calculational Model for the Shear Wave Echo from Subsurface Planar Flaws" *Materials Evaluation*, pp. 46~56.

ASNT, 1991, Nondestructive testing handbook, pp. 551~566.

Date. K and Udagawa. Y., 1989 "Visualization of Ultrasonic waves in a solid by Stroboscopic photoelasticity and Image Processing Techniques," Review of Progress in Quantitative Nondestructive Evaluation. Vol. 8, pp. 1755~1762.

Date. K, Tabata. Y and Shimada. H., 1987, "A Quantitative Evaluation of Ultrasonic Wave in Solid by the Photoelastic Visualization Method" *IEEE Ultrasonic Symposium*, pp. 1093~1097.

Hall, K. G., 1977, "A qualitative evaluation of variable-angle ultrasonic transducers by the photoelastic visualization method" *Ultrasonics*, pp. 245~252.

Hall, K. G., 1982, "Observing ultrasonic wave propagation by stroboscopic visualization method" *Ultrasonics*, pp. 159~167.

Hall, K. G., 1984, "Visualization Technique for the Study of Ultrasonic Wave Propagation in the Railway Industry" *Materials Evaluation*, pp. 922~929.

Harumi, K., 1986, "Computer Simulation of Ultrasonic in a solid" *Material Evaluation*, pp. 1086~1114.

KrautKramer, J. and H., 1990, *Ultrasonic Testing of Materials*, Springer-Verlag, pp. 58~92.

Lee. K. B., 1996, "A study on the characteristics of elastic wave propagation in plates using double pulsed laser holographic interferometry" *KSME*, pp. 3211~3223.

Ludwig, R. and Lord, W., 1986, "Development in the Finite Element Modeling of Ultrasonic NDT Phenomena," *Review of Progress in Quantitative Nondestructive Evaluation*, Vol. 5, pp. 73~81.

Ogilvy, J. A., 1986, "Theoretical comparison of ultrasonic signal amplitudes from smooth and rough defects," *NDT International*, pp. 371~385.

Ogilvy, J. A., 1986, "Ultrasonic beam profiles and beam propagation in an austenitic weld using a theoretical ray tracing model" *Ultrasonic*, pp. 337~347.

Ogilvy, J. A., 1987, "ON THE USE OF FOCUSED BEAMS IN AUSTENITIC WELDS" *British Journal of NDT*, pp. 238 ~246.

Ogilvy, J. A., 1992, "An interactive ray tracing model for ultrasonic nondestructive testing" *NDT International*, pp. 3~10.

Shin, K. B., 1996, "Stress analysis of fir-tree root in turbine rotor using photoelastic technique" *KSME*, pp. 1784~1797.

You, Z and Lord, W., 1989, "Finite Element Study of Elastic Wave Interaction with Cracks," Review of Progress in Quantitative Nondestructive Evaluation, Vol. 8, pp. 109~116.